

Three-dimensional atomic-arrangement reconstruction from an Auger-electron hologram

Tomohiro Matsushita* and Fang Zhun Guo

Japan Synchrotron Radiation Research Institute (JASRI), SPring-8, 1-1-1 Kouto, Sayo-gun, Hyogo 679-5198, Japan

F. Matsui, Yukako Kato, and Hiroshi Daimon

Nara Institute of Science and Technology (NAIST), 8916-5 Takayama, Ikoma, Nara 630-0192, Japan

(Received 18 January 2007; published 13 February 2007)

Current methods for reconstructing three-dimensional atomic arrangements from photoelectron holograms require data sets recorded using multiple incident photon energies. These techniques are thus difficult to apply to Auger-electron holography, since the kinetic energy of the Auger electron is element specific and independent of excitation energy. We propose a scattering pattern extraction algorithm using a maximum-entropy method for reconstructing the three-dimensional atomic arrangement from a single-energy Auger-electron hologram. The algorithm provides a clear atomic image by taking into account the scattering of the electron by nearby atoms and the non- s -wave nature of the Auger electron. We have applied the algorithm to an Auger-electron hologram of Cu(001) recorded at SPring-8's soft x-ray synchrotron radiation beamline BL25SU and succeeded in determining the positions of 102 atoms of the Cu fcc structure.

DOI: 10.1103/PhysRevB.75.085419

PACS number(s): 61.14.-x, 42.40.-i, 79.60.-i

In recent years, x-ray photoelectron diffraction (XPD) and Auger-electron diffraction (AED) have been applied to the study of the structure of solid surfaces and interfaces. The advantages of XPD and AED over standard crystallographic techniques include not only chemical selectivity but also that the short inelastic-scattering length of the emitted electrons makes the diffraction pattern sensitive only to the short-range order of atoms in the vicinity of emitters close to the surface. Both XPD and AED patterns show holographic features.¹ To date several methods for atomic-resolution holography have been proposed, including photoelectron holography,²⁻¹⁵ Auger-electron holography,¹⁶⁻²² diffuse-scattered low-energy electron spectroscopy,²³⁻²⁵ and x-ray fluorescence spectroscopy.²⁶⁻²⁹ Several methods based on Fourier transforms and multienergy photoelectron hologram have been developed. Even if holograms recorded at multiple energies are used, these algorithms can be used to determine the positions of only about ten atoms, since the strong forward-scattering peaks³⁰ and frequency shifts around the forward scattering region hamper the Fourier analysis. It has proven very difficult to reconstruct structures from a single-energy hologram.

The Auger-electron holography has the advantage that cross sections for Auger processes can be larger than those for the direct photoelectron. In addition, there are several possible excitation methods for producing the Auger electrons (photoexcitation, electron-impact excitation, etc.) However, the Auger-electron holography has been neglected in recent years, since the kinetic energy of the Auger electrons is element specific and it is difficult to record holograms produced at different energies and since the kinetic energy of the Auger electrons is independent of the initial excitation energy. In addition, Auger-electron wave functions are not s wave in character,²⁰⁻²² so algorithms based on Fourier transform techniques will not provide clear atomic images.

In this paper, we propose another scattering pattern extraction algorithm (SPEA-MEM), which uses the scattering pattern matrix³¹ and the maximum-entropy method.³² In addition, we have extended the technique to the Auger electron,

which is not s wave in character. The new algorithm can be used to reconstruct atomic arrangements from an Auger-electron hologram recorded at a single electron energy. We demonstrate the effectiveness of the algorithm by applying it to an experimentally observed Cu(001) hologram.

Experiments were performed at SPring-8's BL25SU. High-energy resolution and circularly polarized light in the range of 0.2 to 2 keV are available by using a grating monochromator and twin helical undulator. The Cu(001) surface is cleaned by annealing, and cleanliness is checked by reflection high-energy electron diffraction and x-ray photoemission spectroscopy. An L_3VV Auger-electron hologram of Cu(001) was recorded using the two-dimensional display-type analyzer.³³⁻³⁵ The schematic of the experiment is shown in Fig. 1. The angular distribution of $\pm 55^\circ$ is projected to the screen of the analyzer, and it is measured with charge-coupled device camera. In this experiment, the synchrotron radiation was vertically entered into the sample, and 72 hologram images were measured with rotating the sample in the step of 5° around the axis of light. In this experimental setup, the condition of the crystal and the polarized light does not change because the light is a circularly polarized light. A 2π sr Auger-electron hologram is synthesized by the measured images. The measured 2π sr Auger-electron hologram of Cu(001) L_3VV is shown in Fig. 2(a).

The conventional model of Auger emission is to describe the emitted wave function as incoherent sums over all magnetic quantum number channels m for each angular-momentum channel l , which can be written as²⁰

$$\Phi_L(\vec{k}, \vec{r}) = h_l^{(1)}(|\vec{k}||\vec{r}|)Y_L(\theta, \phi), \quad (1)$$

where \vec{k} is the electron wave vector corresponding to kinetic energy E_k and θ and ϕ represent the emission angles. $L = (lm)$ represents the angular-momentum quantum numbers, $h_l^{(1)}$ is a Hankel function of the first kind, and Y_L is a spherical harmonic.

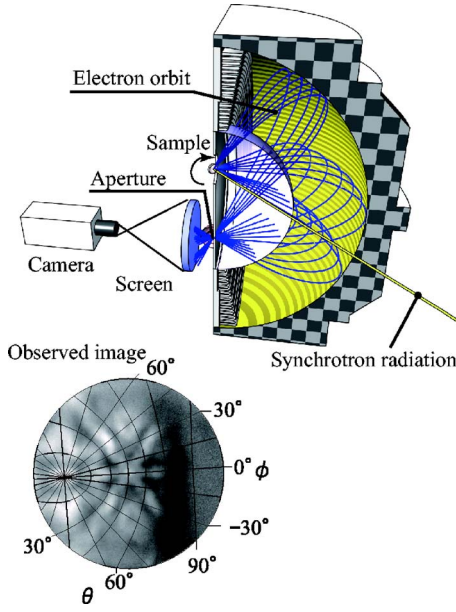


FIG. 1. (Color online) Schematic of the experimental setup and the two-dimensional display-type analyzer. Circularly polarized synchrotron radiation is irradiated onto the sample. The electrons emitted from the sample focus to the aperture by the electric field in the analyzer. The electron that passed the aperture is projected to the screen. Angular distribution without distortion is observed directly on the screen. When the measured image is divided by the penetration function of the analyzer, the clear angular distribution image is obtained. The example of the observed image is shown in figure.

The scattered wave from a scatterer located at position \vec{a} relative to the emitter position can be expressed by $\Psi_{L,\vec{a}}(\vec{k}, \vec{r})$. The interference between the emitter wave and the scattered waves is detected at a detector located far from both atoms, and the emitter and the scattered wave functions at this infinite limit are described as $\Phi_L(\vec{k})$ and $\Psi_{L,\vec{a}}(\vec{k})$. The observed intensity is

$$I(\vec{k}) = \sum_L \left| \Phi_L(\vec{k}) + \sum_h \Psi_{L,\vec{a}_h}(\vec{k}) \right|^2, \quad (2)$$

where h is an index for the scatterer atoms. The hologram function $\chi(\vec{k})$ can then be defined as follows:

$$\chi(\vec{k}) \equiv I(\vec{k}) - I_0(\vec{k}), \quad (3)$$

$$I_0(\vec{k}) \equiv \sum_L |\Phi_L(\vec{k})|^2, \quad (4)$$

where $I_0(\vec{k})$ describes the reference wave intensity. Figures 2(b)–2(f) show the simulated Auger-electron holograms of Cu(001) for s , p , d , f , and g wave functions generated using a cluster of 241 atoms. The patterns show clear differences, and the pattern for an f -wave electron most closely resembles the experimentally observed image of Fig. 2(a), in agreement with the results of Ref. 20.

SPEA-MEM (Ref. 32) is effective reconstructing the atomic arrangements from a single-energy hologram, be-

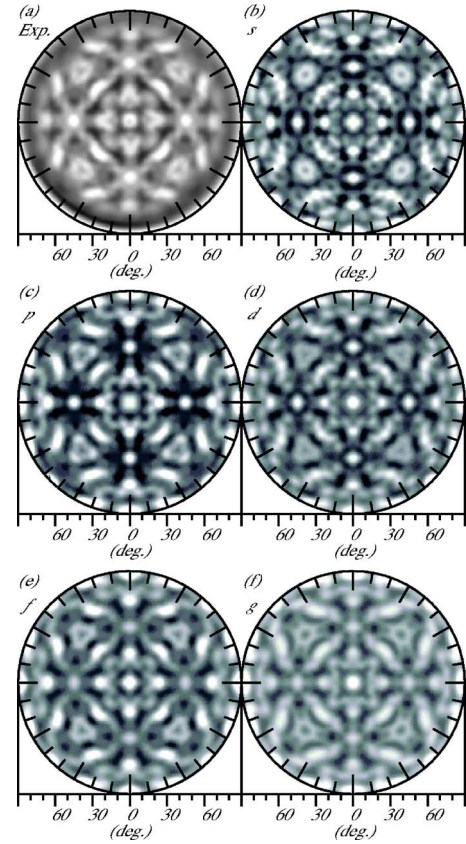


FIG. 2. (Color online) (a) Observed L_3VV Auger-electron hologram of Cu(001) with kinetic energy of 914 eV. [(b)–(f)] Simulated multiple-scattering patterns for emitted waves of s , p , d , f , and g angular momenta for a spherical cluster of 241 atoms. Angular resolution is set to 3° .

cause the elastic-scattering process of the electron is built into the algorithm. In the case of SPEA-MEM for the s wave, the hologram function is approximated by the following expression:

$$\chi(\vec{k}) \approx \frac{\sum_h \hat{t}_{\vec{a}_h}(\vec{k})}{|\vec{a}_h|}, \quad (5)$$

$$\hat{t}_{\vec{a}}(\vec{k}) \equiv |\vec{a}|(|\Psi_{\vec{a}}|^2 + \Phi_0^* \Psi_{\vec{a}} + \text{c.c.}), \quad (6)$$

where Φ_0 is the excited s -wave function and $\Psi_{\vec{a}}$ is the wave function scattered by the scatterer atom located at \vec{a} . The function $\hat{t}_{\vec{a}}(\vec{k})$ defined here describes the pattern caused by a scatterer atom located at \vec{a} normalized by the factor $|\vec{a}|$. Hereafter, $\hat{t}_{\vec{a}}(\vec{k})$ is referred to as the scattering pattern function. The hologram function is expressed by the sum of the scattering pattern functions. However, the Auger-electron hologram is not expressible in this formula, since the Auger electron is described as the incoherent sums over all magnetic quantum number channels.

In the case of the Auger-electron hologram, $\chi(\vec{k})$ can be written as

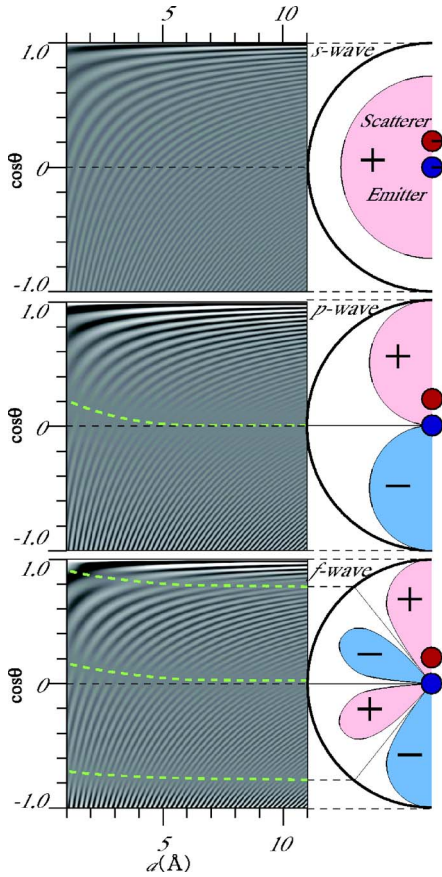


FIG. 3. (Color online) The scattering pattern function $t_{\vec{a}}(\vec{k})$ caused by the scatterer located at $(0,0,a)$, and angular momenta dependence for s -, p -, and f -wave functions of emitter. The vertical axis is defined as $\cos \theta = (\vec{a} \cdot \vec{k}) / |\vec{a}| |\vec{k}|$. The right models depict the emitter and scatterer positions and the polarity of the emitter wave functions.

$$\chi(\vec{k}) \approx \sum_L \left[\sum_h |\Psi_{L,\vec{a}_h}|^2 + \Phi_L^*(\vec{k}) \Psi_{L,\vec{a}_h} + \text{c.c.} \right]. \quad (7)$$

Therefore, we extended the scattering pattern function for the Auger electron as follows:

$$\chi(\vec{k}) = \frac{\sum_h t_{\vec{a}_h}(\vec{k})}{|\vec{a}_h|}, \quad (8)$$

$$t_{\vec{a}_h}(\vec{k}) \equiv |\vec{a}_h| \sum_L (|\Psi_{L,\vec{a}_h}|^2 + \Phi_L^*(\vec{k}) \Psi_{L,\vec{a}_h} + \text{c.c.}). \quad (9)$$

Figure 3 shows the partial scattering pattern functions $t_{\vec{a}}(\vec{k})$ for s -, p -, and f -wave Auger electrons of initial angular momenta (l), which are scattered by a single Cu atom located at a position $(0,0,a)$ relative to the emitter. It can be seen that the pattern is very sensitive to the angular momentum of the emitted electron. For the p -wave electron-scattering pattern a node appears around $\cos \theta = 0$, and the black and white regions of the pattern in the region of $\cos \theta < 0$ are reversed compared to the s -wave pattern. This can be explained by the angular momenta of the reference wave. In the region of

positive $\cos \theta$, the spherical harmonics of p_z are positive and the phase is the same as that of the s wave. On the other hand, in the region of negative $\cos \theta$, the spherical harmonics of p_z are negative, and the black and white stripes are flipped. The p_x and p_y components of the p wave make only a small contribution to the diffraction pattern, since the scatterer atom is located on a node of p_x and p_y and the incident wave is quite weak. A similar discussion can be applied for an f -emitter wave, resulting in the appearance of three nodes in the scattering pattern.

In order to calculate the atomic arrangement from the Auger-electron hologram, the scattering pattern function used by SPEA-MEM is replaced with the extended scattering pattern function for the Auger electron. The hologram signal observed at wave vector \vec{k}_i is denoted as χ_i (with i an integer index), and the array of hologram signals χ_i is defined as χ . A real-space voxel \mathbf{G} , which is an $N \times N \times N$ mesh, to represent real three-dimensional (3D) space is defined, and the value for the voxel located at position vector \vec{a}_j is expressed by G_j (with j an integer index) and represents the distribution in space of scatterers. At the scatterer positions ($\vec{a}_j = \vec{a}_h$), $G_j = 1/|\vec{a}_h|$, and $G_j = 0$ for all other locations. Equation (8) can now be extended as

$$\chi_i = \sum_j t_{\vec{a}_j}(\vec{k}_i) G_j \quad (10)$$

to give the hologram signal. This equation is the simple linear relation,

$$\chi = \mathbf{T}\mathbf{G}, \quad (11)$$

where \mathbf{T} expresses a matrix composed of the scattering pattern functions, with matrix elements $\mathbf{T}_{ij} = t_{\vec{a}_j}(\vec{k}_i)$. Hereafter, this matrix is referred to the scattering pattern matrix. The problem of reconstructing the atomic arrangement now reduces to obtaining the \mathbf{G} given the hologram χ . The number of known data in the $M \times M$ mesh for the Auger-electron hologram is much smaller than the unknown parameters N^3 . This makes the equation difficult to solve using conventional gradient methods. We adopt an iterative-scaling maximum-entropy method for the inverse calculation of the equation. The entropy utilized here is defined as

$$S = - \sum_j G_j^{(n)} \ln \frac{G_j^{(n)}}{G_j^{(n-1)}} - \lambda C, \quad (12)$$

$$C = \frac{1}{N} \sum_i \frac{|\chi_i - (\mathbf{T}\mathbf{G}^{(n)})_i|^2}{\sigma_i^2} - 1, \quad (13)$$

where n is an index for iteration and σ_i is the standard deviation of the noise. The entropy S is maximized to obtain the real-space voxel array \mathbf{G} , i.e., the three-dimensional real-space image.

We have successfully applied the algorithm to the experimentally observed Auger-electron hologram of Cu(001) [Fig. 2(a)]. In order to describe the wave function of the Cu L_3VV Auger electron, the f -wave function is selected in consideration of the selection rule of the transition process of the Auger electron. The vertical slices (xz plane) of the recon-

structed images analyzed using the s - and the f -wave functions are shown in Figs. 4(a) and 4(b). Here, the z axis and the x axis are defined as the surface normal of the sample (the [001] direction) and the [100] direction, respectively. The solid circles represent the scatterer positions. The atomic images show tails along the radial direction. Artifacts are indicated by arrows. The real-space image below the emitter is unclear since the backscattering intensity is much weaker than that of the forward scattering, and the image from the weak backscattering is strongly affected by noise. In the image calculated using an s wave, the image of the first-nearest neighbor is unclear, and there are more artifacts than for the image generated using the f -wave function. The dashed red circles indicate “missing” atomic images. In addition, the region (s) in Fig. 4(b) indicates the position of the shadow of the first-nearest neighbor atom, in which region no atomic images can be seen. This shadow may be caused by multiple-scattering effects, since the first-nearest neighbor atom creates the strongest scattered waves and hence the strongest multiple-scattering effects. Horizontal cross sections (xy plane) of the 3D image at $z=1.8$, 3.6, 5.4, and 7.2 Å generated using an f -wave scattering pattern are shown in Fig. 4(c). The artifacts that remain are mainly due to the tails of atomic images in other layers. The locations of as many as 102 atoms in three-dimensional space have been determined. The size of the reconstructed space size is about 8 Å, and the accuracy of the atomic position is within 0.5 Å for most atoms. Considering the mean free path of the electron, we have succeeded in reconstructing about 80% of the atoms located above the emitter.

In summary, we have developed a SPEA-MEM based on the scattering pattern matrix and an iterative-scaling maximum-entropy method to the Auger-electron wave functions. With it, we have been able to reconstruct up to 102 atomic images in three-dimensional space without the need for any initial atomic structural models. The method enables the determination of the bulk structure around an individual atomic site or impurity by selecting the initial state dependent on the atomic species and chemical state. By selecting the core level of an adsorbate, it is also possible to investigate the surface structure. It is anticipated that the algorithm will become a powerful tool for determining the positions of atomic nuclei around particular target atomic sites.

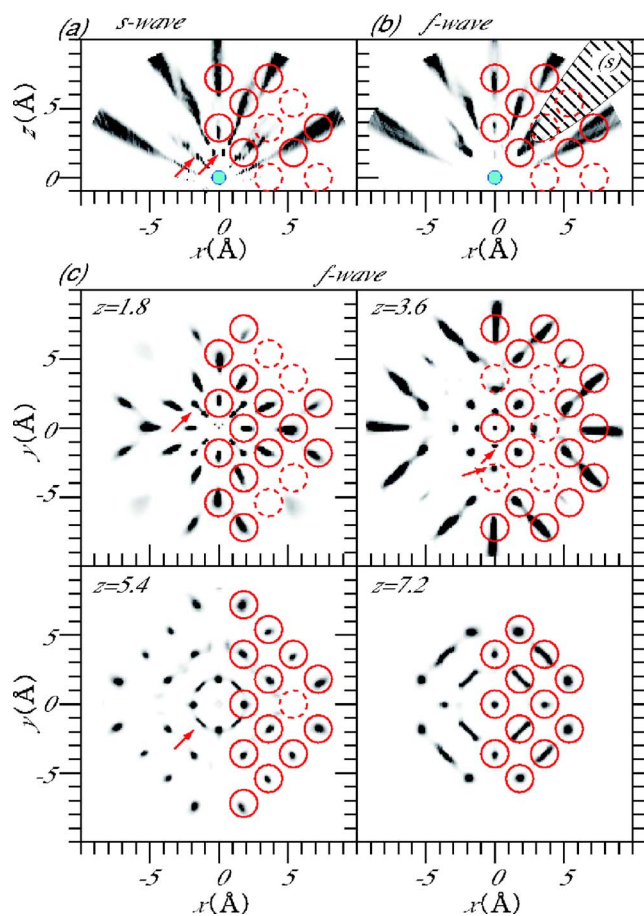


FIG. 4. (Color online) Reconstructed real-space images. (a) and (b) are the vertical slices [(010) plane] of the reconstructed atomic image by using the s -wave and the f -wave functions, respectively. The darkness of the images corresponds to $|a_j|G_j$. The emitter position is indicated by a solid circle. Circles with 1.0 Å radius represent expected positions of Cu atoms, and dashed circles represent atomic positions that are not reconstructed by the calculation. Arrows indicate the position of artifacts. Region (s) reveals a shadow of the first-nearest neighbor atom. (c) The horizontal slices [(001) plane] at various z positions of the reconstructed atomic image by using the f -wave function.

*Electronic address: matusita@spring8.or.jp

¹A. Szöke, *Short Wavelength Coherent Radiation: Generation and Applications*, AIP Conf. Proc. No. 147, (AIP, New York, 1986), p. 361.

²J. J. Barton, Phys. Rev. Lett. **61**, 1356 (1988).

³J. J. Barton, Phys. Rev. Lett. **67**, 3106 (1991).

⁴B. P. Tonner, Zhi-Lan Han, G. R. Harp, and D. K. Saldin, Phys. Rev. B **43**, 14423 (1991).

⁵L. J. Terminello, J. J. Barton, and D. A. Lapiano-Smith, Phys. Rev. Lett. **70**, 599 (1993).

⁶S. Y. Tong, H. Li, and H. Huang, Phys. Rev. Lett. **67**, 3102 (1991).

⁷S. Thevuthasan, G. S. Herman, A. P. Kaduwela, R. S. Saikiv, Y. J. Kim, W. Niemczura, M. Burger, and C. S. Fadley, Phys. Rev. Lett. **67**, 469 (1991).

⁸G. S. Herman, S. Thevuthasan, T. T. Tran, Y. J. Kim, and C. S. Fadley, Phys. Rev. Lett. **68**, 650 (1992).

⁹H. Wu and G. J. Lapeyre, Phys. Rev. B **51**, 14549 (1995).

¹⁰D.-A. Luh, T. Miller, and T.-C. Chiang, Phys. Rev. Lett. **81**, 4160 (1998).

¹¹P. M. Len, J. D. Denlinger, E. Rotenberg, S. D. Kevan, B. P. Tonner, Y. Chen, M. A. Van Hove, and C. S. Fadley, Phys. Rev. B **59**, 5857 (1999).

¹²J. Wider, F. Baumberger, M. Sancbi, R. Gottem, A. Verdini, F.

- Bruno, D. Cvetko, A. Morgante, T. Gerber, and J. Osterwalder, *Phys. Rev. Lett.* **86**, 2337 (2001).
- ¹³S. Omori, Y. Nihei, E. Rotenberg, J. D. Delinger, S. Marchesini, S. D. Kevan, B. P. Tonner, M. A. Van Hove, and C. S. Fadley, *Phys. Rev. Lett.* **88**, 055504 (2002).
- ¹⁴Ph. Hofmann and K.-M. Schindler, *Phys. Rev. B* **47**, 13941 (1993).
- ¹⁵Ph. Hofmann, O. Schaff, and K.-M. Schindler, *Phys. Rev. Lett.* **76**, 948 (1996).
- ¹⁶H. Li and B. P. Tonner, *Phys. Rev. B* **37**, 3959 (1988).
- ¹⁷G. R. Harp, D. K. Saldin, and B. P. Tonner, *Phys. Rev. B* **42**, 9199 (1990).
- ¹⁸S. Y. Tong, C. M. Wei, T. C. Zhao, H. Huang, and H. Li, *Phys. Rev. Lett.* **66**, 60 (1991).
- ¹⁹H. Li, S. Y. Tong, D. Naumović, A. Stuck, and J. Osterwalder, *Phys. Rev. B* **47**, 10036 (1993).
- ²⁰D. K. Saldin, G. R. Harp, and B. P. Tonner, *Phys. Rev. B* **45**, 9629 (1992).
- ²¹T. Greber, J. Osterwalder, D. Naumović, A. Stuck, S. Hüfner, and L. Schlapbach, *Phys. Rev. Lett.* **69**, 1947 (1992).
- ²²D. K. Saldin, G. R. Harp, and X. Chen, *Phys. Rev. B* **48**, 8234 (1993).
- ²³D. K. Saldin and P. L. de Andres, *Phys. Rev. Lett.* **64**, 1270 (1990).
- ²⁴K. Reuter, J. A. Vamvakas, D. K. Saldin, V. Blum, M. Ott, H. Wedler, R. Döll, and K. Heinz, *Phys. Rev. B* **58**, 4102 (1998).
- ²⁵A. Seubert, K. Heinz, and D. K. Saldin, *Phys. Rev. B* **67**, 125417 (2003).
- ²⁶M. Tegze and G. Faigel, *Europhys. Lett.* **16**, 41 (1991).
- ²⁷P. M. Len, S. Thevuthasan, C. S. Fadley, A. P. Kaduwela, and M. A. Van Hove, *Phys. Rev. B* **50**, 11275 (1994).
- ²⁸T. Gog, P. M. Len, G. Materlik, D. Bahr, C. S. Fadley, and C. Sanchez-Hanke, *Phys. Rev. Lett.* **76**, 3132 (1996).
- ²⁹S. Marchesini and C. S. Fadley, *Phys. Rev. B* **67**, 024115 (2003).
- ³⁰C. S. Fadley, *Surf. Sci. Rep.* **19**, 231 (1993).
- ³¹T. Matsushita, A. Agui, and A. Yoshigoe, *Europhys. Lett.* **65**, 207 (2004).
- ³²T. Matsushita, A. Yoshigoe, and A. Agui, *Europhys. Lett.* **71**, 597 (2005).
- ³³H. Daimon, *Rev. Sci. Instrum.* **59**, 545 (1988).
- ³⁴M. Kotsugi *et al.*, *Nucl. Instrum. Methods Phys. Res. A* **467-468**, 1493 (2001).
- ³⁵F. Matsui, H. Daimon, F. Z. Guo, and T. Matsushita, *Appl. Phys. Lett.* **85**, 3737 (2004).